IEEE Access
Multidisciplinary | Rapid Review | Open Access Journal

Received 20 October 2024, accepted 16 November 2024, date of publication 27 November 2024, date of current version 9 December 2024.

Digital Object Identifier 10.1109/ACCESS.2024.3507100

RESEARCH ARTICLE

Fractional Order Sliding Mode Control With GA Tuning for a UAV Quadrotor

NAJIB ALABSARI[1], ABDUL-WAHID A. SAIF[1,2,3], SAMI EL-FERIK[1,2], SALIH DUFFUAA[2,3], AND NABIL DERBEL[4], (Senior Member, IEEE)

[1]Department of Control and Instrumentation Engineering, King Fahd University of Petroleum and Minerals, Dhahran 31261, Saudi Arabia
[2]Interdisciplinary Research Centre for Smart Mobility and Logistics, King Fahd University of Petroleum and Minerals, Dhahran 31261, Saudi Arabia
[3]Industrial and Systems Engineering Department, King Fahd University of Petroleum and Minerals, Dhahran 31261, Saudi Arabia
[4]Electrical Engineering Department, Control and Energy Management Laboratory (CEMLab), University of Sfax, Sfax, Tunisia

Corresponding author: Abdul-Wahid A. Saif (awsaif@kfupm.edu.sa)

This work was supported by the King Fahd University of Petroleum and Minerals through the Interdisciplinary Research Center for Smart Mobility and Logistics under Project INML2414.

ABSTRACT Fractional order calculus (FOC) uses arbitrary order operations in differentiation and integration. Previously, the absence of methods to solve fractional differential equations limited the application of fractional order calculus. However, with the development of new methods, FOC is now applicable in various fields and has been utilized to enhance control system performance in traditional techniques. FOC is used in this study to develop a new fractional structure for the sliding mode control approach that offers improved performance and more robustness to external disturbances. The fractional order sliding mode control (FOSMC) strategy is designed using a Lyapunov-based sliding condition to ensure system stability. To enhance performance, genetic algorithms are used to adjust the fractional orders and controller parameters. The proposed fractional sliding mode control system is applied on an unmanned aerial vehicle system affected by external disturbances and then it is compared with a conventional integer order sliding mode control (IOSMC) system. Simulation results have proved the efficiency of the proposed fractional order controller where it outperforms the conventional sliding mode controller in terms of better transient dynamics and more robustness to external disturbances.

INDEX TERMS Sliding mode control, fractional sliding mode control, unmanned aerial vehicle, genetic algorithm.

I. INTRODUCTION

Fractional order calculus (FOC) is a branch of mathematics that expands the concepts of differentiation and integration to encompass orders beyond just integers. It supports derivatives and integrals of any order (integer, real, or even complex) [1]. As a result of the lack of solution approaches that dealt with fractional differential equations, it was rare to use FOC. Currently, recent advancements have opened doors to FOC application in diverse fields. The theory of fractional calculus has found applications in various engineering disciplines, including mechanical [2, 46], electrical [3], bioengineering [4], and environmental engineering [5]. As a powerful tool for enhancing control system performance, fractional calculus has found its way into various established control structures. This includes fractional order PID control [6], optimal control [7], adaptive control [8], and sliding mode control (SMC) [9]. Studies have demonstrated that fractional order control systems can achieve better performance than integer-order control systems [10].

Driven by their potential to revolutionize fields like logistics, agriculture, and environmental monitoring, the research of unmanned aerial vehicles (UAV) has gained increased focus in the last few years. These versatile aircraft offer valuable tools for both military and civilian applications. In military operations, UAVs are versatile tools, employed for tasks like carrying radar systems, operating cameras, transporting weaponry, and conducting reconnaissance in hostile

The associate editor coordinating the review of this manuscript and approving it for publication was Mohammad Alshabi.

environments. Unmanned aerial vehicles, employed by civilians, contribute to scientific advancements, facilitate life-saving search and rescue missions, track natural resources, and support security tasks [11]. Nowadays, quadrotor UAVS are used widely in agriculture to ensure accurate agricultural production [12]. Several control strategies have been employed to stabilize and control UAVs such as classical and implicit PID controllers [13], [14], linear quadratic regulator (LQR) [15], feedback linearization and adaptive feedback linearization control [16], [17], back stepping [18], sliding mode [19], adaptive fuzzy [20], neural network based MPC [21], in addition to other control approaches [22].

In the literature, the PID and sliding mode control schemes are the most common controllers that have been widely used with fractional structures. In 1994, I. Podlubny [23] introduced the fractional order PID control strategy to control a fractional order system. Then, several fractional order PID controllers were designed using different designs and tuning approaches [24], [25]. The use of FOSMC to stabilize and control UAVs has been studied with employing several fractional schemes to build the control action. In [26] and [27], an integer order sliding surface in addition to a fractional order control action were employed to design the proposed FOSMC. In [28] and [29], the proposed FOSMC is calculated using a fractional sliding surface structure, which incorporates a proportional term and a fractional order derivative term. The authors in [30] proposed a design for a sliding surface, utilizing a fractional-order derivative and integral in addition to an integer-order derivative of the error signal, notably excluding a proportional term. The authors of [31] propose a design for a sliding surface, which utilizes integer and fractional order derivatives of the error term. Researchers in [32] and [33] propose a fractional-order sliding mode control design that utilizes a fractional order manifold. This manifold incorporates both fractional-order derivatives and integrals of the state's error. In [34], the authors designed a fractional-order sliding mode control scheme by employing an integer-order sliding surface in addition to a fractional order switching law.

Genetic algorithms are used as valuable tools for optimizing the control parameters of various controllers. Notably, it has been widely employed to fine-tune the control parameters in fractional order controllers, particularly those used in PID [25], [35] and sliding mode control [36], [37], [38].

The design of fractional order sliding mode control (FOSMC) with a sliding manifold incorporating integral, and fractional-order derivative terms, in addition the proportional term, for controlling UAV altitude and attitude is still not addressed especially with the use of GA to adjust the control parameters. This problem is investigated in this research where a novel fractional-order sliding mode control (FOSMC) scheme is designed for controlling the quadrotor's attitude and altitude dynamics to enhance tracking performance. The approach involves designing a fractional-order sliding manifold, incorporating a proportional term in addition to integer and fractional order derivatives of the tracking error. The FOSMC enhances the vehicle's stability in both altitude and attitude, while a conventional proportional-derivative (PD) controller computes roll and pitch angles to maintain stability along the x and y axes. For the tuning of the designed control system parameters, including fractional orders, a genetic algorithm (GA) is used aiming for improved system performance. A conventional integer-order sliding mode control (IOSMC) system is designed and also tuned using the GA to be compared with the proposed FSCM controller and the comparison results proved that the FSMC controller outperforms the conventional one. A fractional integral term is then added to the fractional sliding surface and the obtained control system is studied and resulted in better performance. The Matlab-Simulink software is utilized for simulating all the systems in this research and the FOMCON toolbox [39] is employed to calculate numerical solutions of the fractional parts.

In this research, section II introduces preliminaries and background on the fractional calculus, UAV mathematical model, and genetic algorithms (GA). Section III explains the derivation and design of the FOSMC system and verifies and compares the results of the designed control approaches through simulations. Section IV presents a comparison between the application of fractional and conventional sliding mode control to Quadrotor where GA is used to optimize the parameters involved in the control scheme. Section V presents the results when adding the fractional integral term to the sliding mode control. Section VI concludes this research.

II. PRELIMINARIES

Fractional calculus is defined by the fundamental operator ${}_aD_t^\alpha$, used for non-integer order differentiation and integration, where α denotes the fractional order which can be a complex number while a and t denote the bounds of the operation. ${}_aD_t^\alpha$ is defined as [23];

$$ {}_aD_t^\alpha = \begin{cases} \dfrac{d^\alpha}{dt^\alpha} : R(\alpha) . > 0; \\ 1 : R(\alpha) . = 0; \\ \displaystyle\int_a^t (d\tau)^\alpha : R(\alpha) < 0 \end{cases} \tag{1} $$

The following definitions are the most commonly utilized for fractional differentiation [40]:

i. Grunwald-Letnikov (GL) definition is given by;

$$ {}_aD_t^\alpha f(t) = \lim_{h\to 0} h^{-\alpha} \sum_{j=0}^{\left[\frac{t-a}{h}\right]} (-1)^j \binom{\alpha}{j} f(t-jh) \tag{2} $$

where [.] represents the integer part.

ii. Riemann-Liouville (RL) definition is given by;

$$ {}_aD_t^{\alpha} f(t) = \frac{1}{\Gamma(n-\alpha)} \frac{d^n}{dt^n} \int_a^t \frac{f(\tau)}{(t-\tau)^{\alpha-n+1}} d\tau; \quad for\ (n-1 < \alpha < n) \tag{3}$$

where $\Gamma(.)$ represents Euler's gamma function.

iii. Caputo definition is given by;

$$ {}_aD_t^{\alpha} f(t) = \frac{1}{\Gamma(n-\alpha)} \int_a^t \frac{f^n(\tau)}{(t-\tau)^{\alpha-n+1}} d\tau; \quad for\ (n-1 < \alpha < n) \tag{4}$$

To ensure full coverage, it is worth noting the utility of the Laplace transform method in addressing fractional order differential equations. Notably, under zero initial conditions, the Laplace transform of the aforementioned fractional order operator for the listed function is given by;

$$ \mathcal{L}\left\{ {}_0D_t^{\alpha} f(t); s \right\} = s^{\alpha} F(s) \tag{5}$$

Nonetheless, there are well-established numerical methodologies exist for evaluating fractional-order derivatives. These encompass Grünwald-Letnikov technique, various continuous and discrete time approximation methods, and the matrix method by Podlubny. Fortunately, certain MATLAB tools serve as valuable assets when employing these methods [40]. Figure 1 shows the difference between integer order (IO) and Riemann-Liouville fractional order (FO) differential and integral of functions $\emptyset(t) = t > 0$.

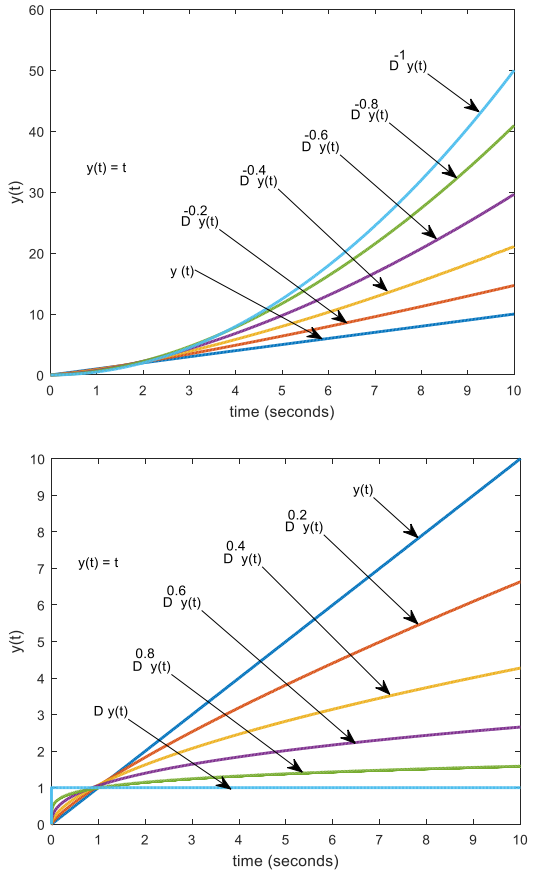

FIGURE 1. Fractional-Order derivative and integral of $y(t)=t$ for different values of β.

A. QUADROTOR'S DYNAMIC MODEL

To determine the quadrotor's dynamic model, two reference frames are considered. One is described by the axes X, Y, and Z (the inertial frame I), and the other is attached to the UAV's center of mass and described by the axes x_B, y_B, and z_B (the body fixed frame B), as shown in Figure 2.

The UAV dynamic model can be obtained based on the Newton-Euler method, with considering the vehicle as a rigid body, as [41] and [42]:

$$ \ddot{x} = \left(\frac{\cos(\varphi)\sin(\theta)\cos(\phi) + \sin(\varphi)\sin(\phi)}{m} \right) u_1 + d_x; \tag{6}$$

$$ \ddot{y} = \left(\frac{\sin(\varphi)\sin(\theta)\cos(\phi) - \cos(\varphi)\sin(\phi)}{m} \right) u_1 + d_y; \tag{7}$$

$$ \ddot{z} = -\mathcal{G} + \left(\frac{\cos(\theta)\cos(\phi)}{m} \right) u_1 + d_z; \tag{8}$$

$$ \ddot{\phi} = \frac{\dot{\varphi}\dot{\theta}(I_{yy} - I_{zz})}{I_{xx}} + \frac{u_2}{I_{xx}} + d_{\phi}; \tag{9}$$

$$ \ddot{\theta} = \frac{\dot{\phi}\dot{\varphi}(I_{zz} - I_{xx})}{I_{yy}} + \frac{u_3}{I_{yy}} + d_{\theta}; \tag{10}$$

$$ \ddot{\varphi} = \frac{\dot{\phi}\dot{\theta}(I_{xx} - I_{yy})}{I_{zz}} + \frac{u_4}{I_{zz}} + d_{\varphi} \tag{11}$$

where I_{xx}, I_{yy} and I_{zz} denote the vehicle moments of inertia about the corresponding axis, $\mathcal{G}$ represents the gravitational constant, m represents the quadrotor mass, (x, y, z) is the position vector, ϕ, θ and φ are the vehicle Euler angles, and u_1, u_2, u_3, u_4 are considered as control signals. The terms d_x, d_y, d_z, d_{ϕ}, d_{θ} and d_{φ} represent perturbation terms of unknown bounds.

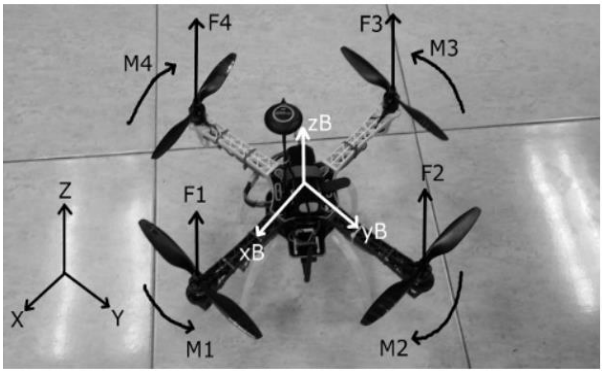

FIGURE 2. The UAV and the coordinate systems [27].

The vehicle is equipped with four rotors that are connected to four motor. Each motor has an angular velocity ω_i, where $(i = 1, 2 \ldots 4)$ and produces a vertical force F_i and moment M_i that are related to ω_i as [43]:

$$ F_i = k_F \omega_i^2, $$
$$ M_i = k_M \omega_i^2, $$

where k_F is the thrust coefficient while k_M is the drag coefficient. The relation between the angular velocities and the control signals, u_i, is [43]:

$$\begin{bmatrix} u_1 \\ u_2 \\ u_3 \\ u_4 \end{bmatrix} = \begin{bmatrix} k_F & k_F & k_F & k_F \\ 0 & lk_F & 0 & -lk_F \\ -lk_F & 0 & lk_F & 0 \\ k_M & -k_M & k_M & -k_M \end{bmatrix} \begin{bmatrix} \omega_1^2 \\ \omega_2^2 \\ \omega_3^2 \\ \omega_4^2 \end{bmatrix}$$

where l denotes the length of the vehicle arm.

B. GENETIC ALGORITHM

Genetic algorithms (GAs) are powerful Heuristic tools that minimize a fitness (cost) function by fine-tuning the parameters of that fitness function. Unlike other methods, to perform their search, The GA techniques need only evolutions of fitness function rather than derivatives or other auxiliary knowledge. Genetic algorithms rely on probabilistic rules rather than deterministic ones, evolving a population of potential solutions for a given problem. These solutions are known as chromosomes or individuals and evolve iteratively. To select the individuals that will produce the next generation, the cost function is used to evaluate the population solutions in a process known as selection, Then the algorithm utilizes crossover and mutation, two essential genetic operators, to produce the next generation of chromosomes. The following steps [44] can summarize the process of genetic algorithm as shown in Figure 3:

- Step 1. Create an initial population of individuals representing potential solutions.
- Step 2. Using the fitness function, measure the performance of each solution.
- Step 3. Choose superior solutions and apply crossover/mutation to generate offspring.
- Step 4. Repeat Iterates (2 and 3) until optimal fitness is reached.

The crossover is a mechanism for chromosomes to share their features by combining the characteristics of two parent individuals to produce offspring. With this process it is possible for good solutions to yield better ones. Mutation is a random change in the composition of a chromosome in a selected individual, occurring with a low probability. This introduces genetic variability within the population, helping to prevent premature convergence and explore new areas of the search space. GA is used here to tune the parameters of the designed control systems, including the fractional orders, aiming to minimize the tracking errors in the quadrotor UAV's position and attitude performance. Thus, each candidate solution (chromosome) within the genetic algorithm is encoded as a vector. This vector holds candidate solutions for the control parameters, including the fractional orders, which act as the ''genes'' of the solution. The performance of each candidate is evaluated by a cost function, where the tracking error is minimized.

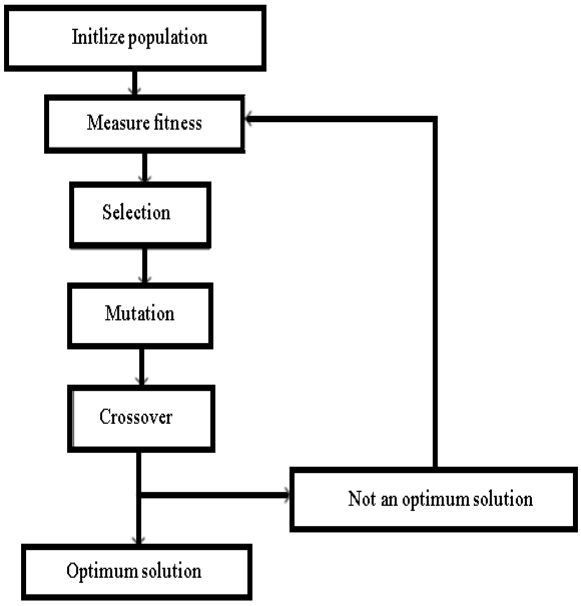

FIGURE 3. Genetic algorithm flow diagram [44].

The cost function is set as the total Integral Absolute Error (IAE).

$$\text{IAE} = \int_0^\infty (|e_x(t)| + |e_y(t)| + |e_z(t)|) \qquad (12)$$

where e_x, e_y and e_z represent the errors of tracking performance in the x, y and z axes, defined as $e_j = j - j_d$ for $j = x, y, z$. The Matlab/Simulink software is employed to implement a genetic algorithm with real-coded chromosomes during control system simulations. The algorithm is implemented with a population size of 50 for chromosomes with 5 or fewer genes and 200 for more than 5 genes. Crossover and mutation probabilities are set to 0.8 and 0.01, respectively. During each iteration, the algorithm calculates the system total Integral Absolute Error (IAE) for the cost function evaluation. The GA is used in the comparison between the conventional and fractional controllers. It is firstly used to tune the control parameters of the conventional control (SMC) and then to tune the control parameters and fractional orders of the FSMC system. Once these parameters are obtained, the conventional and fractional control systems are simulated to compare their results as described in a next section.

III. FRACTIONAL ORDER SLIDING MODE CONTROL (FOSMC)

Assuming that the UAV is under the effect of external perturbations, this section proposes a fractional order sliding mode control (FOSMC) scheme to control and stabilize both the UAV's attitude (Euler angles) and its dynamics in the z direction. Figure 4 shows the proposed control system, which uses two control approaches: FSMC and PD controllers, to control and stabilize the vehicle. While the FSMC controller stabilizes both the quadrotor's attitude and altitude dynamics, the

PD controller calculates the roll (ϕ) and pitch (θ) angles that are needed for the stability of the vehicle position dynamics in both x and y directions.

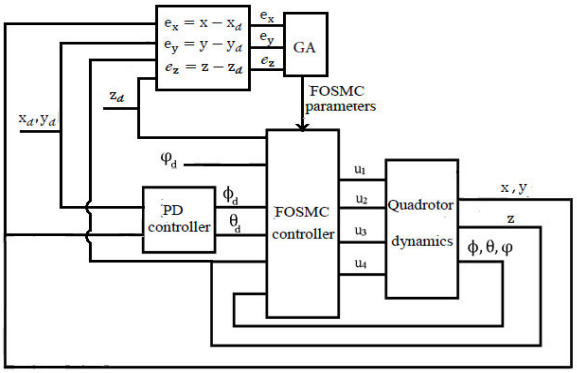

FIGURE 4. Block diagram of the control system.

The results and discussion may be presented separately, or in one combined section, and may optionally be divided into headed subsections.

Assumption: each perturbation signal is unknown but bounded and fulfil the following:

$$\left\|\mathrm{d_j}\right\| \leq \quad \eta_\mathrm{j}\, j = x, y, z, \phi, \theta, \varphi \tag{13}$$

Hence, the terms d_x, d_y, d_z, d_ϕ, d_θ and d_φ in equations (6)-(11) satisfy (13) and represent unspecified disturbance terms with real positive limits η_x, η_y, η_z, η_ϕ, η_θ and η_φ.

A. CONTROL STRATEGY

To control the vehicle altitude dynamics (the dynamics in z direction) which is described by Equation (8), a tracking error $\mathrm{e_z}$ can be defined,

$$e_\mathrm{z} = \mathrm{z} - \mathrm{z}_d \tag{14}$$

where the term $\mathrm{z_d}$ represents a given altitude reference signal. Thus, the proposed sliding manifold ($\mathrm{s_z} = 0$) is chosen such that

$$\mathrm{s_z} = \dot{e}_\mathrm{z} + \rho_\mathrm{z} \mathrm{D}^\alpha e_\mathrm{z} + \lambda_\mathrm{z} e_\mathrm{z} 0 < \alpha < 1 \tag{15}$$

and $\dot{\mathrm{s}}$ can be obtained as:

$$\dot{\mathrm{s}}_\mathrm{z} = \ddot{e}_\mathrm{z} + \rho_\mathrm{z} \mathrm{D}^\alpha \dot{e}_\mathrm{z} + \lambda_\mathrm{z} \dot{e}_\mathrm{z} \tag{16}$$

The parameters ρ_z and λ_z are required to be selected such that the differential equation (15) has a solution that exponentially converges to zero.

$$\ddot{e}_\mathrm{z} = \ddot{\mathrm{z}} - \ddot{\mathrm{z}}_d \tag{17}$$

The FSMC control strategy contains two control parts $\mathrm{u_{11}}$ and $\mathrm{u_{12}}$. The responsibility of $\mathrm{u_{11}}$ is to keep the system on the sliding manifold while responsibility of $\mathrm{u_{12}}$ is to make the system reach the sliding manifold.

Firstly, by considering $\mathrm{d_z} = 0$, the signal $\mathrm{u_{11}}$, that maintain the system on the sliding manifold, is calculated as follows:

substituting (8) in (17)

$$\ddot{e}_\mathrm{z} = -\mathcal{g} + \mathrm{M u_{11}} - \ddot{\mathrm{z}}_d \tag{18}$$

where,

$$\mathrm{M} = \left(\frac{\cos(\phi)\cos(\theta)}{m}\right)$$

Then, substituting (18) in (16)

$$\dot{\mathrm{s}}_\mathrm{z} = -\mathcal{g} + \mathrm{M u_{11}} - \ddot{\mathrm{z}}_\mathrm{d} + \rho_\mathrm{z} \mathrm{D}^\alpha \dot{e}_\mathrm{z} + \lambda_\mathrm{z} \dot{e}_\mathrm{z} \tag{19}$$

Hence $\mathrm{u_{11}}$ can be calculated such that it makes $\dot{\mathrm{s}}_\mathrm{z} = 0$:

$$\mathrm{u_{11}} = \frac{1}{\mathrm{M}} \left(\mathcal{g} + \ddot{\mathrm{z}}_d - \rho_\mathrm{z} \mathrm{D}^\alpha \dot{e}_\mathrm{z} - \lambda_\mathrm{z} \dot{e}_\mathrm{z}\right) \tag{20}$$

Now, for the dynamic system to reach the sliding manifold, an extra control command $\mathrm{u_{12}}$ is required. For this purpose, the following Lyapunov based sliding condition is needed to be satisfied [45]

$$\mathrm{s_z} \dot{\mathrm{s}}_\mathrm{z} \leq -\nu_z \left|\mathrm{s_z}\right| \tag{21}$$

where ν_z represents a positive constant.

Satisfying condition (21) also proves the control system stability. Thus, it is used here to build the controller which guarantees the system stability.

Considering $\mathrm{d_z} \neq 0$, makes $\dot{\mathrm{s}}_\mathrm{z}$ as:

$$\dot{\mathrm{s}}_\mathrm{z} = -\mathcal{g} + \mathrm{M}\left(\mathrm{u_{11}} + \mathrm{u_{12}}\right) + d_\mathrm{z} - \ddot{\mathrm{z}}_d + \rho_\mathrm{z} \mathrm{D}^\alpha \dot{e}_\mathrm{z} + \lambda_\mathrm{z} \dot{e}_\mathrm{z} \tag{22}$$

Substituting from (20) into (22) then multiplying by $\mathrm{s_z}$ gives:

$$\mathrm{s_z} \dot{\mathrm{s}}_\mathrm{z} = \mathrm{s_z M u_{12}} + \mathrm{s_z d_z} \tag{23}$$

which will be satisfied with putting:

$$\mathrm{u_{12}} = \frac{1}{\mathrm{M}} \left(-\sigma_\mathrm{z} \mathrm{sgn}\left(\mathrm{s_z}\right)\right) \tag{24}$$

where $\sigma_\mathrm{z} = \nu_\mathrm{z} + \eta_\mathrm{z}$ and η_z denotes the upper bound of the disturbance signal as in assumption (13).

Substituting from (24) into (23)

$$\mathrm{s_z} \dot{\mathrm{s}}_\mathrm{z} = -\left(\nu_\mathrm{z} + \eta_\mathrm{z}\right) \mathrm{s_z sgn}\left(\mathrm{s_z}\right) + \mathrm{s_z d_z} \tag{25}$$

The term $\mathrm{s_z sgn(s_z)}$ can be replaced by $\left|\mathrm{s_z}\right|$

$$\mathrm{s_z} \dot{\mathrm{s}}_\mathrm{z} = -\nu_\mathrm{z} \left|\mathrm{s_z}\right| - \eta_\mathrm{z} \left|\mathrm{s_z}\right| + \mathrm{s_z d_z} \tag{26}$$

Replacing $\mathrm{s_z}$ and $\mathrm{d_z}$ by $\left|\mathrm{s_z}\right| \mathrm{sgn}\left(\mathrm{s_z}\right)$ and $\left|\mathrm{d_z}\right| \mathrm{sgn}\left(\mathrm{d_z}\right)$ respectively leads to:

$$\begin{aligned} \mathrm{s_z} \dot{\mathrm{s}}_\mathrm{z} = -\nu_\mathrm{z} \left|\mathrm{s_z}\right| - \left|\mathrm{s_z}\right| \left(\eta_\mathrm{z}\right. \\ \left. + \mathrm{sgn(s_z) sgn(d_z)} \left|\mathrm{d_z}\right|\right) \end{aligned} \tag{27}$$

Thus, if the signs of $\mathrm{s_z}$ and $\mathrm{d_z}$ are similar, we obtain:

$$\begin{aligned} \mathrm{s_z} \dot{\mathrm{s}}_\mathrm{z} &= -\nu_\mathrm{z} \left|\mathrm{s_z}\right| - \left(\eta_\mathrm{z} + \left|\mathrm{d_z}\right|\right) \left|\mathrm{s_z}\right| \\ &\leq -\nu \left|\mathrm{s_z}\right| \end{aligned} \tag{28}$$

and, if their signs are different, we have:

$$\mathrm{s_z} \dot{\mathrm{s}}_\mathrm{z} = -\nu_\mathrm{z} \left|\mathrm{s_z}\right| - \left(\eta_\mathrm{z} - \left|\mathrm{d_z}\right|\right) \left|\mathrm{s_z}\right| \tag{29}$$

Since η_z is the bound of the disturbance signal d_z, as in (13), thus:

$$|d_z| \leq \eta_z$$

which makes:

$$s_z \dot{s}_z = -\nu_z |s_z| - (\eta_z - |d_z|)|s_z| \leq -\nu |s_z| \quad (30)$$

From (28) and (30), (21) is always satisfied.

Since $u_1 = u_{11} + u_{12}$, thus, from (20) and (24),

$$u_1 = \frac{1}{M}(N_z + \mathcal{G}) = \frac{m}{\cos(\phi)\cos(\theta)}(\mathcal{P}_z + \mathcal{G}) \quad (31)$$

where

$$N_z = \ddot{z}_d - \rho_z D^{\alpha} \dot{e}_z - \lambda_z \dot{e}_z - \sigma_z \text{sgn}(s_z) \quad (32)$$

In order to design the control inputs u_2 and u_3, ϕ_d and θ_d are defined as the desired reference roll and pitch angles respectively and the small angle approximation is used to model the system. Therefore, equations (6, 7, 9, and 11) are expressed as:

$$\ddot{x} \approx \tan(\theta)(N_z + \mathcal{G}) + d_x; \quad (33)$$

$$\ddot{y} \approx -\tan(\phi)(N_z + \mathcal{G}) + d_y; \quad (34)$$

$$\ddot{\phi} = \frac{u_2}{I_{xx}} + d_\phi; \ddot{\theta} = \frac{u_3}{I_{yy}} + d_\theta; \ddot{\varphi} = \frac{u_4}{I_{zz}} + d_\varphi \quad (35)$$

To determine the necessary angles ϕ_d and θ_d to achieve convergence of tracking errors e_x and e_y to zero, the terms $\tan(\phi)$ and $\tan(\theta)$ are selected as virtual inputs in (33) and (34) respectively. Subsequently e_x and e_y are defined as:

$$e_x = x - x_d . e_y = y - y_d . \quad (36)$$

where the terms x_d and y_d are given reference signals in x and y directions respectively. Supposing d_x and d_y are zeros, a PD controller can be designed as:

$$\theta_d = \tan^{-1}\left(\frac{1}{N_z + \mathcal{G}}(\ddot{x}_d - K_{dx}\dot{e}_x - K_{px}e_x)\right) \quad (37)$$

$$\phi_d = -\tan^{-1}\left(\frac{1}{N_z + \mathcal{G}}(\ddot{y}_d - K_{dy}\dot{e}_y - K_{py}e_y)\right) \quad (38)$$

where $K_{dx}.K_{px}.K_{dy}$ and K_{py} are the PD control parameters and should be selected to achieve exponential convergence of e_x and e_y to zero.

It should be noticed that, for e_x and e_y to converge exponentially to zero, angles θ and ϕ are required to approach the calculated θ_d and ϕ_d as soon as possible. Therefore, the control inputs u_2 and u_3 are required to be designed for that purpose. The same strategy of designing u_1 is utilized again for designing the control inputs u_2, u_3 and u_4. The fractional manifolds are now defined as:

$$s_i = \dot{e}_i + \rho_i D^{\alpha} e_i + \lambda_i e_i = 0 \quad (39)$$

$$e_i = i - i_d, i = \phi, \theta, \varphi \quad (40)$$

By repeating the same process of designing u_1, the input signals u_2, u_3 and u_4 are found as

$$u_2 = I_{xx}(\ddot{\phi}_d - \rho_\phi D^{\alpha}\dot{e}_\phi - \lambda_\phi \dot{e}_\phi - \sigma_\phi \text{sgn}(s_\phi)); \quad (41)$$

$$u_3 = I_{yy}(\ddot{\theta}_d - \rho_\theta D^{\alpha}\dot{e}_\theta - \lambda_\theta \dot{e}_\theta - \sigma_\theta \text{sgn}(s_\theta)); \quad (42)$$

$$u_4 = I_{zz}(\ddot{\varphi}_d - \rho_\varphi D^{\alpha}\dot{e}_\varphi - \lambda_\varphi \dot{e}_\varphi - \sigma_\varphi \text{sgn}(s_\varphi)). \quad (43)$$

B. SIMULATION RESULTS WITHOUT USING GA

In this part, the designed control strategy is evaluated using MATLAB-Simulink software. The system is simulated with applying the FOSMC scheme on the UAV model in Equations 6-11, using the control signals given in Equations 31, 41-43.

The simulated quadrotor system has a mass (m) of 1.4 kg and moments of inertia I_{xx}, I_{yy} and I_{zz} of 0.02 kg.m^2, 0.02 kg.m^2, and 0.04 kg.m^2 respectively. The controllers parameters are selected through trial and error as indicated in Table 1.

TABLE 1. The FOSMC and PD control parameters.

rameters	FOSM Parameters		
$K_{px} = 30$	$\lambda_z = 1$	$\sigma_z = 10$	$\rho_z = 7$
$K_{dx} = 5$	$\lambda_\phi = 1$	$\sigma_\phi = 1.5$	$\rho_\phi = 1$
$K_{py} = 30$	$\lambda_\theta = 1$	$\sigma_\theta = 1.5$	$\rho_\theta = 1$
$K_{dy} = 5$	$\lambda_\varphi = 1$	$\sigma_\varphi = 10$	$\rho_\varphi = 7$

To study the efficiency of the proposed FOSMC system, reference and perturbation signals are applied on the system at different times. Firstly, when $t = 1s$, a reference input of unit step in z direction is imposed to be followed by the system. Then, when $t = 10s$, two signals of sinusoidal form are applied as references to be tracked in x and y directions as:

$$x_{\text{ref}} = y_{\text{ref}} = P\sin(\omega t) \quad (44)$$

where P =1 [m], while $\omega = 0.086 * \pi$ [s^{-1}]. The reference of angle φ is defined as:

$$\varphi_{\text{ref}} = 0$$

To prevent excessively high derivative values, low pass filters are used to filter these reference signals. The applied reference signals are shown in figure 5.

When $t = 23s$, external disturbance signals are applied on the system as:

$$d = k_a + k_b \sin(\frac{2\pi t}{T_1}) \quad (45)$$

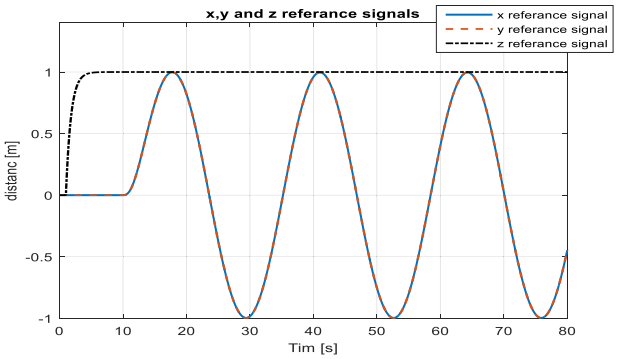

FIGURE 5. The applied reference signals in x, y and z directions.

The parameters k_a, k_b and T_1 are set as follows:

$$k_a = 0.1\left[\frac{\text{rad}}{\text{s}^2}\right], k_b = 0.01, T_1 = 1.8\ sec.$$

The perturbation terms in equations (6)-(11) are taken as:

$$d_x = d_y = d_z = 0;$$
$$d_\phi = d_\theta = d_\varphi = d$$

Throughout the system simulation, saturation functions are employed to enforce the control inputs to be within predefined limits to ensure safe and stable operation of the system. The specific limits applied are [0 30], [−10 10], and [−10 10] for u_1, u_2 and u_3, respectively. To compute the required numerical solutions, the Matlab ode45 solver is used during the simulation of the proposed control system. The numerical calculations of the fractional parts are handled using the FOMCON toolbox. The sgn function is applied here as:

$$\text{sgn(s)} = \frac{s}{|s| + c}$$

The value of c is a tiny positive constant, specifically set as: $c = 0.005$.

Figures 6-8 show simulation results of the designed fractional control system (FOSMC) with different values of the orders (α). Figure 6 shows the system tracking performances, whereas figures 7 and 8 demonstrate the system' tracking error and the control inputs, respectively. These results illustrate that deferent fractional orders lead to deferent behaviors with achieving better performance at lower α values. It can be noted that, using higher values of the fractional order α, result in slower transient dynamics where both raise and settling times increase. It also results in lower robustness against the applied external perturbations. Additionally, the figures demonstrate that higher values of α cause higher initial input efforts when applying sinusoidal reference signals in both x and y directions. Nevertheless, the proposed fractional control structure accomplished the tracking tasks efficiently.

These Figures show that, the best performance is achieved with α set at 0.1. Nevertheless, varying the fractional order produces varied system responses. Thus, the genetic algorithm will be employed in the following section to tune the control parameters including the fractional orders α's in order to accomplish better response.

IV. COMPARISON BETWEEN THE FRACTIONAL AND CONVENTIONAL SLIDING MODE CONTROL

In order to assess the proposed fractional sliding mode control strategy, it will be compared here with the conventional sliding mode approach. First, the conventional controller can be obtained by following the same steps of deriving the fractional one that is reported in the previous section, except that the sliding services are introduced as

$$\text{s}_\text{j} = \dot{e}_\text{j} + \lambda_\text{j}\text{e}_\text{j} \quad = 0, j = z, \phi, \theta, \varphi \tag{46}$$

Therefore, the resulted control inputs will take the forms:

$$\text{u}_1 = \frac{m}{\cos(\phi)\cos(\theta)}\left(\text{N}_\text{z} + g\right) \tag{47}$$

where:

$$\text{N}_\text{z} = \ddot{\text{z}}_\text{d} - \lambda_\text{z}\dot{e}_\text{z} - \sigma_\text{z}\text{sgn}(\text{s}_\text{z}); \tag{48}$$
$$\text{u}_2 = \text{I}_{xx}(\ddot{\phi}_\text{d} - \lambda_\phi\dot{e}_\phi - \sigma_\phi\text{sgn}(\text{s}_\phi)); \tag{49}$$
$$\text{u}_3 = \text{I}_{yy}(\ddot{\theta}_\text{d} - \lambda_\theta\dot{e}_\theta - \sigma_\theta\text{sgn}(\text{s}_\theta)); \tag{50}$$
$$\text{u}_4 = \text{I}_{zz}(\ddot{\varphi}_\text{d} - \lambda_\varphi\dot{e}_\varphi - \sigma_\varphi\text{sgn}(\text{s}_\varphi)) \tag{51}$$

The PD controller described by equations (37) and (38) is utilized to obtain the roll and pitch angles that are needed for the stability of the position dynamics in both x and y axes.

A. SIMULATION RESULTS WITH USING GA

In this section the proposed FOSMC system is compared with conventional IOSMC system using the Matlab Simulink environment. The quadrotor system is first simulated using the conventional sliding mode control approach. Then, the resulting performance is compared with simulations of the proposed FOSMC technique.

Unlike the fractional control system that simulated in subsection (-B-III-B) which was supposed to have the same fractional order α for all the included fractional manifolds, the system here is designed with different fractional order for each fractional manifold. The GA is employed to adjust the control parameters for both conventional and fractional control systems. For the conventional system the GA is used to tune the parameters λ_z, λ_ϕ, λ_θ and λ_φ. This means that each chromosome in the population contains these four genes. For the fractional system, the GA is used to tune the parameters λ_z, λ_ϕ, λ_θ, λ_φ, ρ_z, ρ_ϕ, ρ_θ and ρ_φ along with the fractional orders α_z, α_ϕ, α_θ, and α_φ making up a total of twelve genes in each chromosome. Other parameters are used as in the previous simulation subsection (BIII-B) and the fitness function (12) is used to evaluate all the solutions. The process of adjusting the FOSMC parameters is achieved by following the GA steps described in subsection (II-B) where step 2 includes simulating the system to calculate the errors then measuring performance of each solution using the fitness function. Figure 9 depicts the convergence behavior of the IAE error function of the FOSMC system,

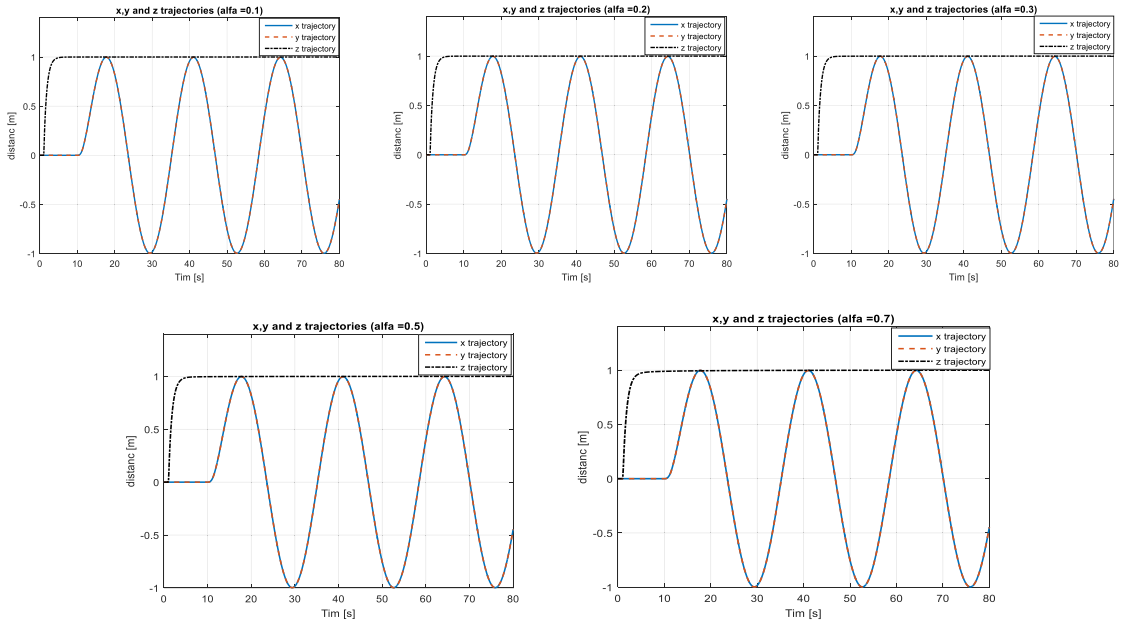

FIGURE 6. The system tracking performance with different values of α.

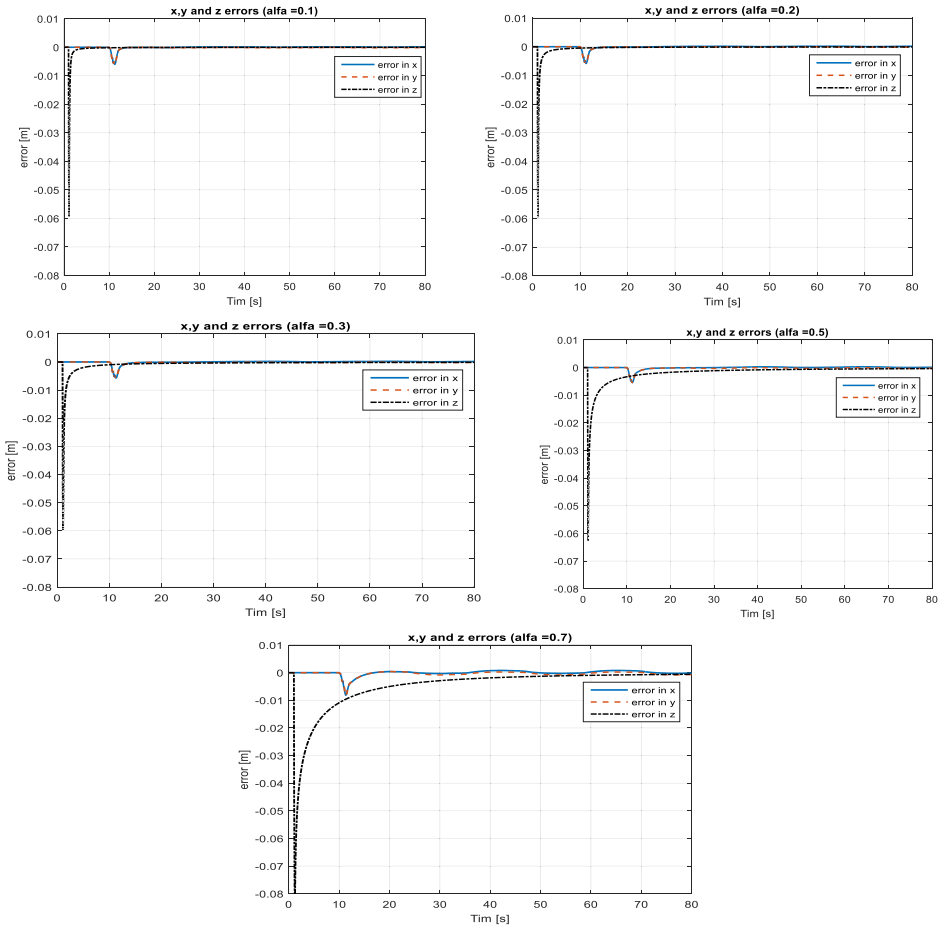

FIGURE 7. The system tracking errors with different values of α.

illustrating the evolution of its fitness value as the number of generations progresses. As evident from the figure, the FOSMC error function exhibits a clear trend of convergence, effectively reaching a stable fitness value after

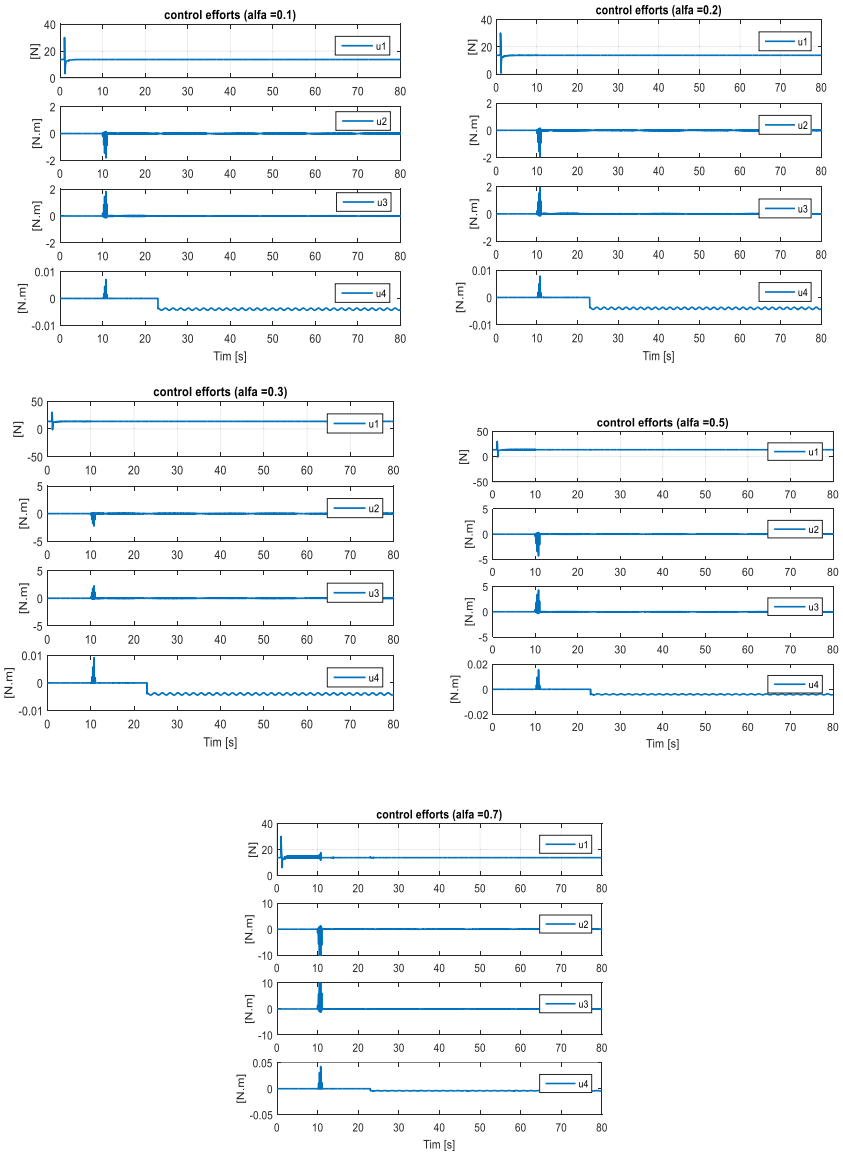

FIGURE 8. The system control efforts with changing the order α.

approximately eight generations. This observation suggests that the algorithm has successfully identified a near-optimal solution within a reasonable timeframe. While there might be slight fluctuations in the fitness value beyond this point, the overall trend indicates that the algorithm has reached a point of diminishing returns, and further generations are unlikely to yield significant improvements. The same GA steps are applied to both control techniques with no difference except that the FSOMS approach have more control parameters. The tuned fractional orders α_j are constrained to the range [0.01, 0.9], while the remaining parameters ($\boldsymbol{\lambda}, \boldsymbol{\rho}, \boldsymbol{\mu}$) are limited to the interval [1], [10]. Table 2 shows the GA-tuned parameters. These parameters are used to obtain the simulation results that will be used to compare the systems.

TABLE 2. The tuned control parameterss (ρ, λ, α).

Convectional control para meters	Fractional control parameters		
$\lambda_z = 9$	$\lambda_z = 1.65$	$\rho_z = 1.15$	$\alpha_z = 0.05$
$\lambda_\phi = 4.58$	$\lambda_\phi = 4.23$	$\rho_\phi = 3.88$	$\alpha_\phi = 0.02$
$\lambda_\theta = 4.49$	$\lambda_\theta = 4.98$	$\rho_\theta = 4.61$	$\alpha_\theta = 0.02$
$\lambda_\varphi = 8.82$	$\lambda_\varphi = 5.57$	$\rho_\varphi = 3.31$	$\alpha_\varphi = 0.05$

As shown in Figure 10, a similar form of the reference signals that were used in subsection (-B-III-B) will be used

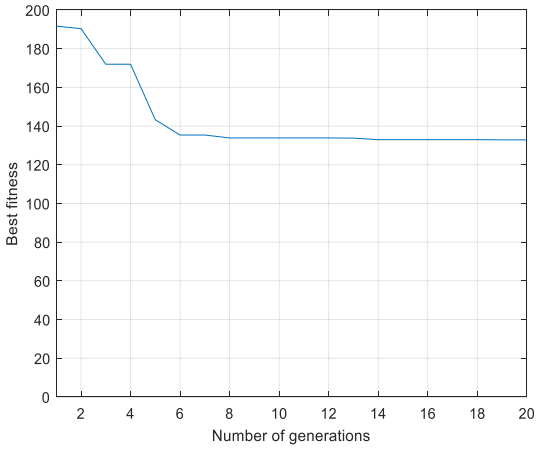

FIGURE 9. The change of best fitness values with increasing no. of generations for the FOSMC.

here. The difference here is that the x and y sinusoidal reference signals start earlier (at t=1s) with higher frequency, and the parameters values of the perturbation parameters are increased to obtain:

$$\begin{aligned} &Z_{ref} = unit\ step\ signal; \\ &\mathrm{X_{ref}} = \mathrm{Y_{ref}} = \mathrm{A}\sin(0.127\pi\,\mathrm{t})\,[\mathrm{m}]\,; \\ &\varphi_{\mathrm{ref}} = 0 \end{aligned} \tag{52}$$

A=1 [m]; and

$$\begin{aligned} &\mathrm{d_l} = 0.5 + 0.04\sin\left(\frac{2\pi\,\mathrm{t}}{1.8}\right)\left[\frac{\mathrm{rad}}{\mathrm{s}^2}\right]; \\ &\mathrm{d_x} = \mathrm{d_y} = \mathrm{d_z} = 0; \\ &\mathrm{d}_\phi = \mathrm{d}_\theta = \mathrm{d}_\varphi = \mathrm{d_l} \end{aligned} \tag{53}$$

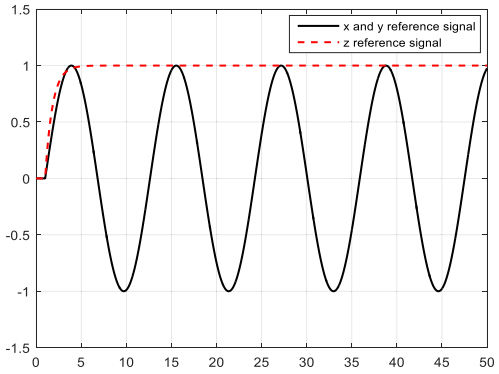

FIGURE 10. The input reference signals (sinusoidal).

Throughout the simulations of the systems, saturation functions are employed to enforce the control inputs to be within predefined limits to ensure safe and stable operation of the system. The specific limits applied are [0 30], [−10 10], and [−10 10] for u_1, u_2 and u_3, respectively. To compute the required numerical solutions, the Matlab ode45 solver is used during the simulation of the proposed control system. The numerical solutions of the fractional parts are calculated using the FOMCON toolbox.

Figure 11 shows the system's tracking trajectories in the x, y, and z directions for both controllers. Equations 31, 32, 41, 42, and 43 are used as control inputs to plot the response of the FOSMC system while equations 47-51 are used to control and obtain the response of the conventional integer order sliding mod control system.

It is clear that, in both cases the quadrotor system achieves the required tracking tasks. However, Figure 12, Figure 13 and Figure 14, which compare the tracking errors of both controllers in the x, y, and z directions, show better performance and more robustness when applying the proposed FOSMC. Figure 12 shows the tracking errors of both controllers in the x direction while Figure 13 shows their tracking error in the y direction. Both figures show that the conventional control system results in high deviations from the required paths during the transient period and responds to the applied perturbation signals with large oscillations around the required paths. However, these figures clearly demonstrate that the fractional order control system shows smaller deviations with less response to the perturbations and more robustness than the conventional one. Figure 14 shows the tracking errors of both controllers in the z direction. The fitness function (IAE), described in equation (12), also proves that the proposed fractional system outperforms the conventional one where it equals 193.76 m for the conventional system while it is equal to 132.95 m for the fractional system. Figure 15 shows a comparison between the errors of the Euler angles (ϕ, θ and φ) for both control systems. It demonstrates that the Euler angles errors of the fractional order system converge to zero faster than those of the conventional system.

These figures show that the proposed fractional sliding mode controller achieved better results than the conventional sliding mode controller in terms of robustness against external perturbations and improving the tracking performance during the transient period. In fact the tunable fractional orders add more degree of freedom and flexibility to tune the controller what expand the search space and in sequence increase the possibility to find better results and better performance.

V. PRELIMINARIES EFFECT OF ADDING FRACTIONAL INTEGRAL (I^β)

So far, the control strategy has been implemented with considering a sliding manifold without including any integral term. In this section the fractional control method is designed with considering that the fractional sliding manifolds include an additional term which has a fractional integral structure (I^β). Firstly, it is well known that the integral I^β term can be written as a derivative term in the form $D^{-\beta}$. By adding fractional integrator terms to the sliding manifolds, they can be defined as:

$$\mathrm{s_j} = \dot{\mathrm{e}}_\mathrm{j} + \rho_\mathrm{j}\mathrm{D}^\alpha\mathrm{e_j} + \mu_\mathrm{j}\mathrm{D}^{-\beta}\mathrm{e_j} + \lambda_\mathrm{j}\mathrm{e_j} = 0; j = z, \phi, \theta, \varphi \tag{54}$$

where $0 < \beta < 1$

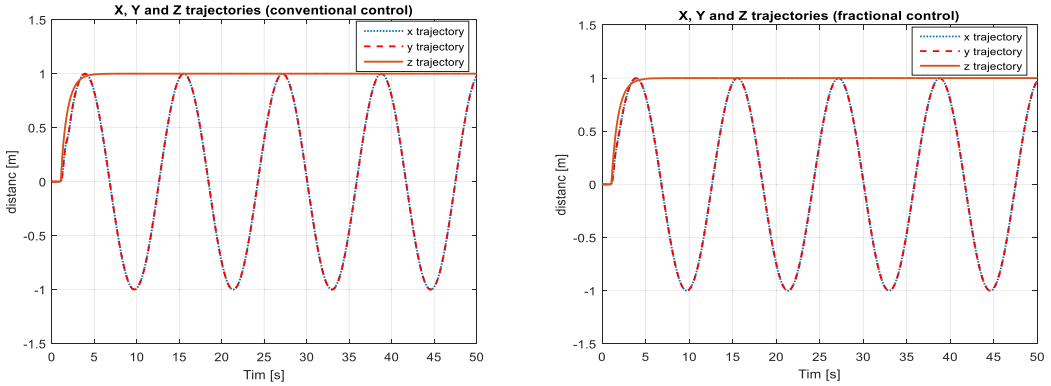

FIGURE 11. The performance of both the conventional and fractional sliding mode control.

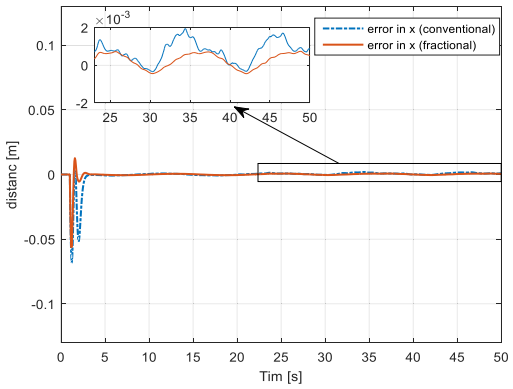

FIGURE 12. The tracking error in x direction of both conventional and fractional SMC.

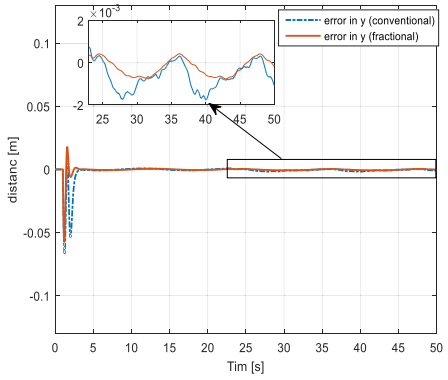

FIGURE 13. The tracking error in y direction for both conventional and fractional SMC.

By following the same procedure in subsection (III-A) to compute the control signals, we obtain:

$$u_1 = \frac{m}{cos\,(\phi)\,cos\,(\theta)}\,(N_z+g) \tag{55}$$

where

$$N_z = \ddot{z}_d - \rho_z D^{\alpha}\dot{e}_z - \mu_z D^{-\beta}\dot{e}_z - \lambda_z \dot{e}_z - \sigma_z \mathrm{sgn}(s_z); \tag{56}$$

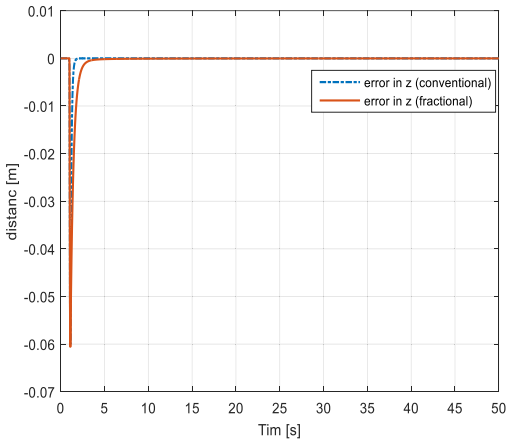

FIGURE 14. The tracking error in z-direction of both conventional and fractional SMC.

and

$$u_2 = I_{xx}(\ddot{\phi}_d - \rho_\phi D^{\alpha}\dot{e}_\phi - \mu_\phi D^{-\beta}\dot{e}_\phi - \lambda_\phi \dot{e}_\phi - \sigma_\phi \mathrm{sgn}(s_\phi)); \tag{57}$$

$$u_3 = I_{yy}(\ddot{\theta}_d - \rho_\theta D^{\alpha}\dot{e}_\theta - \mu_\theta D^{-\beta}\dot{e}_\theta - \lambda_\theta \dot{e}_\theta - \sigma_\theta \mathrm{sgn}(s_\theta)); \tag{58}$$

$$u_4 = I_{zz}(\ddot{\varphi}_d - \rho_\varphi D^{\alpha}\dot{e}_\varphi - \mu_\varphi D^{-\beta}\dot{e}_\varphi - \lambda_\varphi \dot{e}_\varphi - \sigma_\varphi \mathrm{sgn}(s_\varphi)); \tag{59}$$

A. SIMULATION RESULTS WITH USING GA

To evaluate the fractional-order sliding mode control system with adding the fractional integral term in the sliding manifold, the fractional control system is simulated with considering the control input signals in equations (55)-(59) to control the system.

The same reference signals shown in Figure 10 which were used in subsection (IV-A) will be used here as reference signals such that we can study the effect of adding the integral term.

Therefore,

$$Z_{ref} = unit\ step\ signal;$$

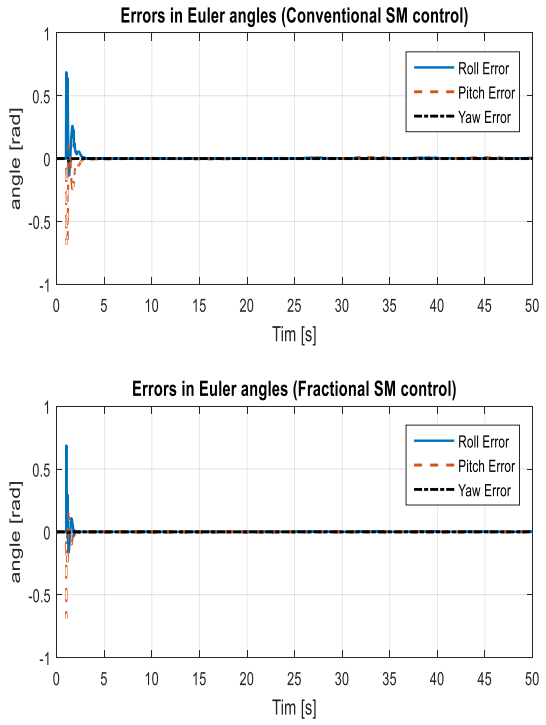

FIGURE 15. Euler angles errors of both the conventional and fractional sliding mode control.

TABLE 3. GA tuned control parameters ($\lambda, \rho, \alpha, \mu, \beta$).

λ_z =1.4	ρ_z = 1.53	α_z = 0.1	μ_z = 3.11	β_z = 0.02
λ_ϕ =4.1	ρ_ϕ = 1.81	α_ϕ = 0.02	μ_ϕ = 4.94	β_ϕ = 0.5
λ_θ =3.8	ρ_θ =1.2	α_θ = 0.05	μ_θ = 4.84	β_θ = 0.2
λ_φ = 9.61	ρ_φ =8.5	α_φ =0.1	μ_φ = 6.61	β_ϕ = 0.1

$$X_{ref} = Y_{ref} = 1 * sin(0.127\pi t)\,[m]\,;$$
$$\varphi_{\text{ref}} = 0$$

Moreover, the same perturbation signals are also used as:

$$d_\phi = d_\theta = d_\varphi = 0.5 + 0.04\sin(\frac{2\pi t}{1.8})[\text{rad/s}^2]$$

To avoid obtaining too high derivative values, low pass filters are used to filter all reference signals. The same GA process that is conducted in subsection (IV-A) is used here with more eight genes ($\mu_z, \mu_\phi, \mu_\theta, \mu_\varphi, \beta_z, \beta_\phi, \beta_\theta$, and β_φ) for each chromosome as shown in Table 3. The tuned fractional orders are constrained to the range [0.01, 0.9], while the remaining parameters ($\boldsymbol{\lambda}, \boldsymbol{\rho}, \boldsymbol{\mu}$) are limited to the interval [1], [10]. The results of applying the GA tuning are shown in Table 3.

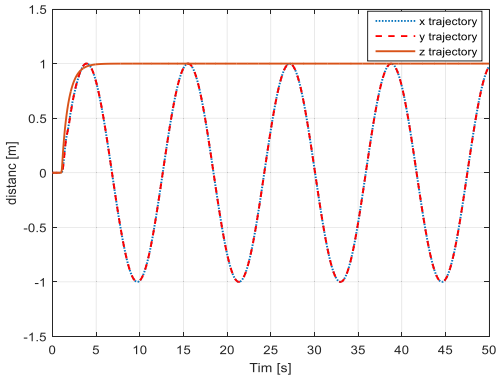

FIGURE 16. The system performance (with adding I^β term).

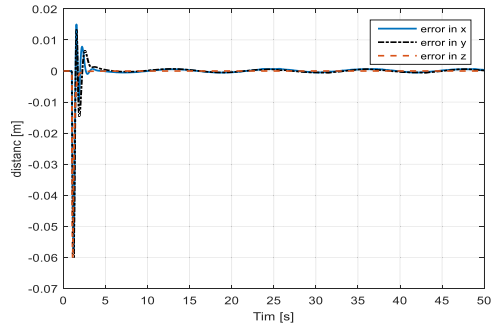

FIGURE 17. The tracking errors (with adding I^β term).

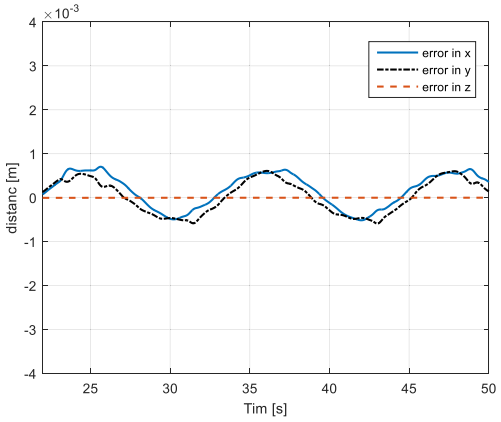

FIGURE 18. Zoomed tracking errors (by adding I^β term).

By adding an integral term to the fractional sliding manifolds, the performance of the control system gains more improvement than in the case of only proportional and derivative terms.

Figure 16 and Figure 17 show the tracking performance and errors of the fractional controller when adding the I^β term. The system achieves the task of following the reference signals (X_{ref}, Y_{ref} and Z_{ref}) efficiently. Figure 18 and Figure 19 show zoomed illustrations for the tracking errors of the fractional control case with adding I^β term and the case without it respectively. Figure 20 shows the Euler errors

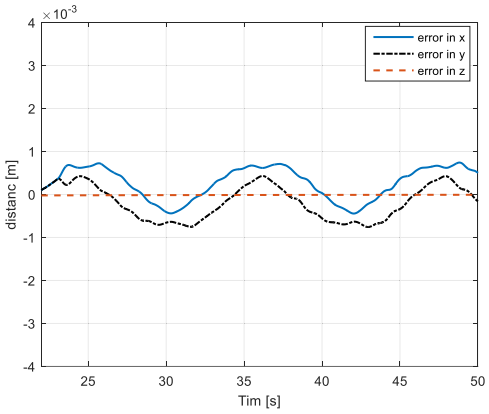

FIGURE 19. Zoomed tracking errors (without I^{β} term).

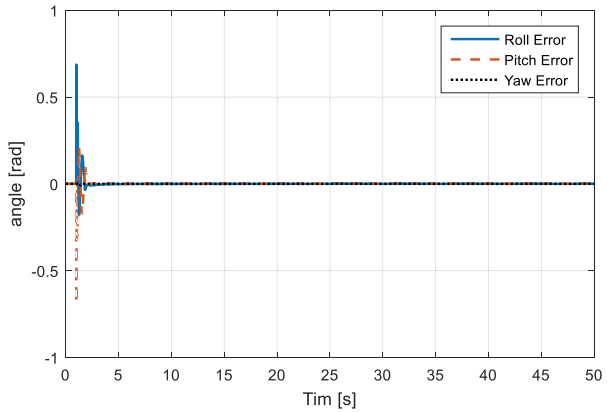

FIGURE 20. The Euler errors (when adding I^{β} term).

with adding I^{β} term. These figures show an improvement in terms of robustness against external perturbations in the case of adding the I^{β} term to the fractional control. The total IAE in this case is equal to 125.94 m which is better than 132.95 m of the case without I^{β} term.

This leads to the conclusion that adding a fractional integral term to the sliding manifold achieved better performance than the obtained results with only proportional and derivative terms.

VI. CONCLUSION

This paper proposed a novel fractional-order sliding mode control (FOSMC) approach for stabilizing and controlling the nonlinear model of a UAV quadrotor subject to external disturbances. The FOSMC effectively regulates the attitude and altitude dynamics, while a conventional PD controller manages the roll and pitch angles, ensuring the quadrotor's stability in tracking accuracy. Finally, a genetic algorithm effectively tunes the control parameters with the fractional orders in the FOSMC systems, for optimized system performance based on a predefined fitness function. The extension of this work to heterogeneous multi-agent systems is under consideration.

REFERENCES

[1] A. W. Saif, N. Alabsari, S. E. Ferik, and M. Elshafei, "Formation control of quadrotors via potential field and geometric techniques," *Int. J. Adv. Appl. Sci.*, vol. 7, no. 6, pp. 82–96, Jun. 2020, doi: 10.21833/ijaas.2020.06.011.

[2] J. Li and Y. Li, "Dynamic analysis and PID control for a quadrotor," in *Proc. IEEE Int. Conf. Mechatronics Autom.*, Aug. 2011, pp. 573–578.

[3] S. Wang, A. Polyakov, and G. Zheng, "Quadrotor stabilization under time and space constraints using implicit PID controller," *J. Franklin Inst.*, vol. 359, no. 4, pp. 1505–1530, Mar. 2022, doi: 10.1016/j.jfranklin.2022.01.002.

[4] E. Okyere, A. Bousbaine, G. T. Poyi, A. K. Joseph, and J. M. Andrade, "LQR controller design for quad-rotor helicopters," *J. Eng.*, vol. 2019, no. 17, pp. 4003–4007, Jun. 2019.

[5] M. Alejandro Lotufo, L. Colangelo, and C. Novara, "Feedback linearization for quadrotors UAV," 2019, *arXiv:1906.04263*.

[6] A. Eltayeb, M. F. Rahmat, and M. A. Mohd Basri, "Adaptive feedback linearization controller for stabilization of quadrotor UAV," *Int. J. Integr. Eng.*, vol. 12, no. 4, pp. 1–17, Apr. 2020.

[7] O. García, P. Ordaz, O.-J. Santos-Sánchez, S. Salazar, and R. Lozano, "Backstepping and robust control for a quadrotor in outdoors environments: An experimental approach," *IEEE Access*, vol. 7, pp. 40636–40648, 2019.

[8] H. Rios, R. Falcon, O. A. Gonzalez, and A. Dzul, "Continuous sliding-mode control strategies for quadrotor robust tracking: Real-time application," *IEEE Trans. Ind. Electron.*, vol. 66, no. 2, pp. 1264–1272, Feb. 2019, doi: 10.1109/TIE.2018.2831191.

[9] C. Li, Y. Wang, and X. Yang, "Adaptive fuzzy control of a quadrotor using disturbance observer," *Aerosp. Sci. Technol.*, vol. 128, Sep. 2022, Art. no. 107784, doi: 10.1016/j.ast.2022.107784.

[10] B. Jiang, B. Li, W. Zhou, L.-Y. Lo, C.-K. Chen, and C.-Y. Wen, "Neural network based model predictive control for a quadrotor UAV," *Aerospace*, vol. 9, no. 8, p. 460, Aug. 2022.

[11] T. P. Nascimento and M. Saska, "Position and attitude control of multi-rotor aerial vehicles: A survey," *Annu. Rev. Control*, vol. 48, pp. 129–146, May 2019.

[12] L. Di, "Cognitive formation flight in multi-unmanned aerial vehicle-based personal remote sensing systems," Utah State Univ., 2021. [Online]. Available: https://digitalcommons.usu.edu/etd/985

[13] O. Khatib, "Real-time obstacle avoidance for manipulators and mobile robots," *Int. J. Robot. Res.*, vol. 5, no. 1, pp. 90–98, Mar. 1986.

[14] X. Li, D. Zhu, and Y. Qian, "A survey on formation control algorithms for multi-AUV system," *Unmanned Syst.*, vol. 2, no. 4, pp. 351–359, Oct. 2014.

[15] R. Matušu, "Application of fractional order calculus to control theory," *Int. J. Math. Model. Methods Appl. Sci.*, vol. 5, no. 7, pp. 1162–1169, 2011.

[16] A. Tepljakov, E. Petlenkov, and J. Belikov, "FOPID controller tuning for fractional FOPDT plants subject to design specifications in the frequency domain," in *Proc. Eur. Control Conf. (ECC)*, Jul. 2015, pp. 3502–3507.

[17] M. H. Heydari, M. R. Hooshmandasl, F. M. Maalek Ghaini, and C. Cattani, "Wavelets method for solving fractional optimal control problems," *Appl. Math. Comput.*, vol. 286, pp. 139–154, Aug. 2016.

[18] Z. M. Odibat, "Adaptive feedback control and synchronization of non-identical chaotic fractional order systems," *Nonlinear Dyn.*, vol. 60, no. 4, pp. 479–487, Jun. 2010.

[19] J. Wang, C. Shao, and Y.-Q. Chen, "Fractional order sliding mode control via disturbance observer for a class of fractional order systems with mismatched disturbance," *Mechatronics*, vol. 53, pp. 8–19, Aug. 2018, doi: 10.1016/j.mechatronics.2018.05.006.

[20] Y. Chen, I. Petras, and D. Xue, "Fractional order control—A tutorial," in *Proc. Amer. Control Conf.*, Jun. 2009, pp. 1397–1411, doi: 10.1109/ACC.2009.5160719.

[21] C. Izaguirre-Espinosa, A. J. Muñoz-Vazquez, A. Sanchez-Orta, V. Parra-Vega, and I. Fantoni, "Fractional-order control for robust position/yaw tracking of quadrotors with experiments," *IEEE Trans. Control Syst. Technol.*, vol. 27, no. 4, pp. 1645–1650, Jul. 2019, doi: 10.1109/TCST.2018.2831175.

[22] H. Farbakhsh, M. Tavakoli-Kakhki, H. D. Taghirad, R. Azarmi, and F. Padula, "Fractional order fast terminal sliding mode controller design with finite-time convergence: Application to quadrotor UAV," in *Proc. 26th IEEE Int. Conf. Emerg. Technol. Factory Autom. (ETFA)*, Sep. 2021, pp. 1–8, doi: 10.1109/etfa45728.2021.9613288.

[23] M. Labbadi and M. Cherkaoui, "Adaptive fractional-order nonsingular fast terminal sliding mode based robust tracking control of quadrotor UAV with Gaussian random disturbances and uncertainties," *IEEE Trans. Aerosp. Electron. Syst.*, vol. 57, no. 4, pp. 2265–2277, Aug. 2021, doi: 10.1109/TAES.2021.3053109.

[24] M. Labbadi and H. E. Moussaoui, "An improved adaptive fractional-order fast integral terminal sliding mode control for distributed quadrotor," *Math. Comput. Simul.*, vol. 188, pp. 120–134, Oct. 2021, doi: 10.1016/j.matcom.2021.03.039.

[25] M. Labbadi, Y. Boukal, M. Cherkaoui, and M. Djemai, "Fractional-order global sliding mode controller for an uncertain quadrotor UAVs subjected to external disturbances," *J. Franklin Inst.*, vol. 358, no. 9, pp. 4822–4847, Jun. 2021, doi: 10.1016/j.jfranklin.2021.04.032.

[26] M. Pouzesh and S. Mobayen, "Event-triggered fractional-order sliding mode control technique for stabilization of disturbed quadrotor unmanned aerial vehicles," *Aerosp. Sci. Technol.*, vol. 121, Feb. 2022, Art. no. 107337, doi: 10.1016/j.ast.2022.107337.

[27] M. Labbadi, A. J. Muñoz-Vázquez, M. Djemai, Y. Boukal, M. Zerrougui, and M. Cherkaoui, "Fractional-order nonsingular terminal sliding mode controller for a quadrotor with disturbances," *Appl. Math. Model.*, vol. 111, pp. 753–776, Nov. 2022, doi: 10.1016/j.apm.2022.07.016.

[28] S. El-Ferik, M. Maaruf, F. M. Al-Sunni, A. A. Saif, and M. M. Al Dhaifallah, "Reinforcement learning-based control strategy for multi-agent systems subjected to actuator cyberattacks during affine formation maneuvers," *IEEE Access*, vol. 11, pp. 77656–77668, 2023, doi: 10.1109/ACCESS.2023.3296741.

[29] Z. Ma, Z. Liu, P. Huang, and Z. Kuang, "Adaptive fractional-order sliding mode control for admittance-based telerobotic system with optimized order and force estimation," *IEEE Trans. Ind. Electron.*, vol. 69, no. 5, pp. 5165–5174, May 2022.

[30] H. Saribas and S. Kahvecioglu, "PSO and GA tuned conventional and fractional order PID controllers for quadrotor control," *Aircr. Eng. Aerosp. Technol.*, vol. 93, no. 7, pp. 1243–1253, Sep. 2021.

[31] H. L. Maurya, L. Behera, and N. K. Verma, "Trajectory tracking of quad-rotor UAV using fractional order PI$\wedge\mu$ D$\wedge\lambda$ controller," in *Computational Intelligence: Theories, Applications and Future Directions*. Cham, Switzerland: Springer, 2019, pp. 171–186.

[32] H. Delavari, R. Ghaderi, A. Ranjbar, and S. Momani, "Fuzzy fractional order sliding mode controller for nonlinear systems," *Commun. Nonlinear Sci. Numer. Simul.*, vol. 15, no. 4, pp. 963–978, Apr. 2010.

[33] S. Labdai, L. Chrifi-Alaoui, S. Drid, L. Delahoche, and P. Bussy, "Real-time implementation of an optimized fractional sliding mode controller on the quanser-aero helicopter," in *Proc. Int. Conf. Control, Autom. Diagnosis (ICCAD)*, Oct. 2020, pp. 1–6.

[34] A. Tepljakov, "FOMCON: Fractional-order modeling and control toolbox," in *Fractional-order Modeling and Control of Dynamic Systems*. Cham, Switzerland: Springer, 2017, pp. 107–129.

[35] I. Petres, *Fractional Derivatives, Fractional Integrals, and Fractional Differential Equations in Matlab*. London, U.K.: IntechOpen, 2011.

[36] A. Govea-Vargas, R. Castro-Linares, M. A. Duarte-Mermoud, N. Aguila-Camacho, and G. E. Ceballos-Benavides, "Fractional order sliding mode control of a class of second order perturbed nonlinear systems: Application to the trajectory tracking of a quadrotor," *Algorithms*, vol. 11, no. 11, p. 168, Oct. 2018, doi: 10.3390/a11110168.

[37] M. J. Reinoso, L. I. Minchala, P. Ortiz, D. F. Astudillo, and D. Verdugo, "Trajectory tracking of a quadrotor using sliding mode control," *IEEE Latin Amer. Trans.*, vol. 14, no. 5, pp. 2157–2166, May 2016.

[38] D. Mellinger. (2012). *Trajectory Generation and Control For Quadrotors Daniel Mellinger*. [Online]. Available: https://repository.upenn.edu/handle/20.500.14332/32133

[39] A. Jayachitra and R. Vinodha, "Genetic algorithm based PID controller tuning approach for continuous stirred tank reactor," *Adv. Artif. Intell.*, vol. 2014, pp. 1–8, Dec. 2014, doi: 10.1155/2014/791230.

[40] J.-J. E. Slotine and W. Li, *Applied Nonlinear Control*, vol. 199. Upper Saddle River, NJ, USA: Prentice-Hall, 1991.

[41] O. Alburaiki, "Leader-follower slam based navigation and fleet management control," King Fahd Univ. Petroleum Minerals KSA, 2012. [Online]. Available: http://eprints.kfupm.edu.sa/id/eprint/138817

[42] Z. Yu, Y. Zhang, B. Jiang, C.-Y. Su, J. Fu, Y. Jin, and T. Chai, "Fractional-order adaptive fault-tolerant synchronization tracking control of networked fixed-wing UAVs against actuator-sensor faults via intelligent learning mechanism," *IEEE Trans. Neural Netw. Learn. Syst.*, vol. 32, no. 12, pp. 5539–5553, Dec. 2021.

[43] Z. Yu, Y. Zhang, B. Jiang, C.-Y. Su, J. Fu, Y. Jin, and T. Chai, "Refined fractional-order fault-tolerant coordinated tracking control of networked fixed-wing UAVs against faults and communication delays via double recurrent perturbation FNNs," *IEEE Trans. Cybern.*, vol. 2, no. 3, pp. 1–13, Apr. 2022.

[44] Z. Yu, Y. Zhang, B. Jiang, C.-Y. Su, J. Fu, Y. Jin, and T. Chai, "Enhanced recurrent fuzzy neural fault-tolerant synchronization tracking control of multiple unmanned airships via fractional calculus and fixed-time prescribed performance function," *IEEE Trans. Fuzzy Syst.*, vol. 30, no. 10, pp. 4515–4529, Oct. 2022.

[45] B. Wang, W. Chen, B. Zhang, P. Shi, and H. Zhang, "A nonlinear observer-based approach to robust cooperative tracking for heterogeneous spacecraft attitude control and formation applications," *IEEE Trans. Autom. Control*, vol. 68, no. 1, pp. 400–407, Jan. 2023.

NAJIB ALABSARI received the B.Sc. degree from the Mechatronics Department, Baghdad University, Iraq, and the M.S. and Ph.D. degrees in systems and control engineering from the Control and Instrumentation Engineering Department, King Fahd University of Petroleum and Minerals, Dhahran, Saudi Arabia. His research interests include control of mobile robotics and unmanned aerial vehicles, intelligent control systems, multi-agent and cooperative control, robust control, and optimization and heuristic algorithms.

ABDUL-WAHID A. SAIF received the B.Sc. degree from the Physics Department, King Fahd University of Petroleum and Minerals, Dhahran, Saudi Arabia, the M.Sc. degree from the Systems Engineering (SE) Department, King Fahd University of Petroleum and Minerals, and the Ph.D. degree from the Control and Instrumentation Group, Department of Engineering, Leicester University, Leicester, U.K. He was a Research Assistant with the SE Department, King Fahd University of Petroleum and Minerals, a Lecturer with the Electrical Engineering Department, King Fahd University of Petroleum and Minerals, and a Lecturer with the Physics Department, King Fahd University of Petroleum and Minerals. He is currently a Professor of control and instrumentation with the SE Department, King Fahd University of Petroleum and Minerals. After finishing the Ph.D. degree, he joined the SE Department, King Fahd University of Petroleum and Minerals. He taught several courses in modeling and simulation, digital control, digital systems, microprocessor and microcontrollers in automation, optimization, numerical methods, PLC's, process control, and control system design. He has published more than 115 articles, patents, book chapters, and technical reports in reputable journals and conferences. His research interests include simultaneous and strong stabilization, robust control and H8-optimization, instrumentation, and computer control.

SAMI EL-FERIK received the B.Sc. degree in electrical engineering from Laval University, Québec City, QC, Canada, and the M.Sc. and Ph.D. degrees in electrical and computer engineering from Polytechnique Montréal, Canada. After the completion of the Ph.D., and Post-Doctoral positions, he was with the Research and Development Center of Systems, Controls, and Accessories, Pratt and Whitney, Canada. He is currently a Professor in control and instrumentation engineering at King Fahd University of Petroleum and Minerals. He is also the Founding Director of the Interdisciplinary Research Center for Smart Mobility and Logistics. His research interests include sensing, monitoring, multiagent systems, and nonlinear control, swarm robotics, vision-based navigation, vision intelligence, with strong multidisciplinary research, and applications.

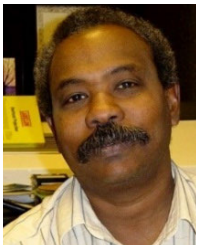

SALIH DUFFUAA received the Ph.D. degree in operations research from The University of Texas at Austin. He is currently a Professor of industrial engineering and operations research with the Industrial and Systems Engineering Department, King Fahd University of Petroleum and Minerals, Dhahran, Saudi Arabia. He has published extensively. His work has appeared in journals, such as *Journal of Optimization Theory and Applications*, *European Journal of Operational Research*, *Engineering Optimization*, *Operational Research*, *International Journal of Production Research*, and *International Journal of Quality and Reliability Management*. He won the Excellence in Research Award three times and the Excellence in Teaching Award three times at the King Fahd University of Petroleum and Minerals. He is the Editor-in-Chief of the *Journal of Quality in Maintenance Engineering*, published by Emerald in the U.K.

NABIL DERBEL (Senior Member, IEEE) was born in Sfax, Tunisia, in April 1962. He received the Engineering Diploma degree from the École Nationale d'Ingénieurs de Sfax (ENIS), Tunisia, in 1986, the Diplôme d'Etudes Approfondies degree in automatic control from the Institute National des Sciences Appliquées de Toulouse, France, in 1986, the Doctorat d'Université degree from the Laboratoire d'Automatique et d'Analyse des Systèmes, Toulouse, France, in 1989, and the Doctorat d'État degree from the Ecole Nationale d'Ingénieurs de Tunis (ENIT), Tunisia. He joined Tunis University, in 1989, where he has been involved in research and education in different positions. Since 2003, he has been a Full Professor of electrical engineering. He is the author or co-author of more than 90 articles published in international journals and more than 500 papers published in national and international conferences. His current research interests include optimal control, sliding mode control, sensors, robotic systems, intelligent methods, instrumentation, and renewable energies.